Journal of Materials Chemistry B

ROYAL SOCIETY OF CHEMISTRY

PAPER

View Article Online
View Journal | View Issue

Cite this: J. Mater. Chem. B, 2025, 13, 3049

Synthesis and characterization of poly(ester amide)-based materials for 3D printing of tissue engineering scaffolds†

Patrícia dos Santos,[ab] Beatriz Alves,[a] Sara Inocêncio,[a] Pedro Nunes,[a] Stephen M. Richardson,[c] Antonio Gloria,[d] Arménio Serra,[a] Ana Clotilde Fonseca‡*[a] and Marco Domingos ‡*[b]

The fabrication of three-dimensional (3D) scaffolds with imprinted physical, chemical and topographical cues is instrumental in tissue engineering strategies to instruct cell function and guide the regeneration of tissues. α-Amino acids based poly(ester amide)s (AAA-PEAs), combining the biocompatibility and biodegradability of polyesters with the superior mechanical properties of polyamides, have emerged as promising scaffolding materials. However, their processing *via* extrusion-based 3D printing remains challenging due to the lack of polymeric structures with suitable molecular weight and thermal stability. Here, we develop a new library of high molecular weight AAA-PEAs based on L-alanine (PEA-ala), L-alanine/glycine (PEA-ala–gly (75 : 25)) and L-alanine/glycine/jeffamine (PEA-ala–gly–jeff (50 : 25 : 25)) and investigate their performance as polymeric materials for 3D printing against commercially available poly(ε-caprolactone) (PCL). Thermogravimetric analysis reveals the stability of AAA-PEAs at high temperatures, enabling their processing *via* melt-extrusion printing. Despite differences in complex viscosity between PCL and AAA-PEAs, highlighted by oscillatory rheology measurements, the printability of AAA-PEAs does not seem to be compromised, resulting in 3D scaffolds with good shape-fidelity. Additional physicochemical characterisation of synthesised materials also confirm the possibility of fabricating two-dimensional (2D) films and 3D scaffolds with different mechanical properties, wettability and degradation profiles, depending on the AAA-PEA used. Biological tests carried out *in vitro* confirm the ability of synthesised materials to support the adhesion and function of metabolically active human bone marrow derived mesenchymal stem cells (hBM-MSCs). The newly synthesised AAA-PEAs expand the range of processable materials *via* melt-extrusion and contribute to the fabrication of scaffolds with tuneable physicochemical properties for improved tissue regeneration.

Received 3rd October 2024,
Accepted 26th January 2025

DOI: 10.1039/d4tb02220c

rsc.li/materials-b

1. Introduction

Scaffold-guided tissue regeneration strategies have shown great promise in restoring the structure and function of human tissues damaged by trauma or disease. However, the regeneration process is complex and very much dependent on the synergistic integration of cells, biomolecules and biomaterial scaffolds.[1–3] The latter play a crucial role in supporting cell adhesion, cell proliferation, and inducing cell differentiation through different chemical and physical cues.[1,3,4] Biocompatibility and biodegradability are essential properties but to successfully promote new tissue ingrowth and maturation, scaffolds must also comply with other numerous requirements including mechanical, topographical and biological.[4–6] In terms of scaffold fabrication, additive manufacturing (AM) also known as three-dimensional (3D) printing, offers unique advantages over "conventional" techniques such as

[a] CEMMPRE, ARISE, Department of Chemical Engineering, University of Coimbra, Rua Sílvio Lima-Polo II, 3030-790, Coimbra, Portugal. E-mail: p.santos0495@gmail.com, biadalves77@gmail.com, sara.i.r.inocencio@gmail.com, pedroecn@hotmail.com, armenio.serra@gmail.com, anafs@eq.uc.pt

[b] Department of Mechanical and Aerospace Engineering, School of Engineering, Faculty of Science and Engineering & Henry Royce Institute, The University of Manchester, M13 9PL, Manchester, UK. E-mail: marco.domingos@manchester.ac.uk

[c] Manchester Cell-Matrix Centre, Division of Cell Matrix Biology and Regenerative Medicine, School of Biological Sciences, Faculty of Biology, Medicine and Health, Manchester Academic Health Sciences Centre, The University of Manchester, M13 9PL, Manchester, UK. E-mail: s.richardson@manchester.ac.uk

[d] Department of Industrial Engineering, University of Naples Federico II, P.le Tecchio 80, 80125, Naples, Italy. E-mail: angloria@unina.it

† Electronic supplementary information (ESI) available. See DOI: https://doi.org/10.1039/d4tb02220c

‡ These authors contributed equally as last authors.

electrospinning, freeze-drying, thermally induced phase separation (TIPS), solvent casting, and gas foaming.[7,8] Operating in a layer-by-layer manner, 3D printing allows for the computer-controlled deposition of multiple materials to generate scaffolds with tailored internal/external architectures to accommodate different cell types, induce specific cellular responses and ultimately guide the regeneration of the targeted tissue.[9,10] 3D printing is an umbrella term for a vast selection of AM technologies typically used in the fabrication of scaffolds for tissue engineering (TE). Depending on the scaffolding material and tissue application, it is possible to choose between extrusion-based, vat photopolymerization, powder bed fusion and material jetting systems.[2] Extrusion-based printing is undoubtedly the most used technique due to the flexibility offered in terms of the number and type of processable materials, cost and ease of operation.[11,12] In terms of processable biomaterials, aliphatic polyesters, such as poly(ε-caprolactone) (PCL), poly(L-lactic acid) (PLA) and poly(D,L-lactic-*co*-glycolic acid) (PLGA) are among the most popular used in extrusion-based printing. These polymers offer good thermal processability and stability but tend to display poor bioactivity and trigger immunological reactions when implanted *in vivo*.[13–15] Significant efforts have been made in recent years to address some of these challenges and improve cell–material interactions, typically through post-printing functionalization[16] or blending with other materials.[16–19] However, these methods can be time-consuming and result in unwanted changes to the scaffold's properties. α-Amino acid-based poly(ester amide)s (AAA-PEAs), combining the biodegradability of ester bonds (–COO–) with the excellent thermal and mechanical properties of amide bonds (–NHCO–), are increasingly recognised as alternative materials for 3D printing.[20–22]

The versatility of their polymeric structures allows for the fabrication of scaffolds with tuneable physicochemical, biological and mechanical properties, a critical aspect when attempting to replicate the structural and functional organization of native human tissues. The presence of α-amino acids enhance cell–matrix interactions[23,24] and enables *in vivo* degradation. The latter generates both acidic and basic products, thus avoiding the significant pH drop commonly observed in the degradation of polyesters.[20] Interestingly, few studies on 3D printing of AAA-PEAs exist in the literature.[24,25] We have previously reported the formulation of PCL and PEA blends for melt-extrusion printing and demonstrated that the addition of PEA strongly enhanced hydrophilicity, mechanical response and cellular function of PCL scaffolds.[25] More recently, Ansari *et al.* used a similar fabrication technique to investigate the application of glycine-based PEA as polymeric materials for AM and TE.[24] Despite relatively high processing temperatures (approx. 200 °C) and significant number of crystalline domains, which could negatively impact their biodegradation behavior, the authors reported the successful fabrication and osteogenic potential of PEA-based scaffolds for bone tissue regeneration. Building on the work of Ansari *et al.* we propose a new and expanded library AAA-PEAs with tuneable physical and chemical properties for 3D printing of scaffolds for guided tissue regeneration. The synthesis of AAA-PEAs was carried out *via* active solution polycondensation, and AAA-PEAs with three distinct structures were prepared, *viz.* L-alanine based PEA (PEA-ala), L-alanine and glycine based PEA (PEA-ala–gly) and a L-alanine, glycine and jeffamine based PEA (PEA-ala–gly–jeff). The presence of the α-amino acids aimed primarily at improving the overall biodegradability and biocompatibility of the PEAs. Jeffamine, a polyether-based diamine, was selected to further increase the hydrophilicity of PEAs, since this is a characteristic often desired for TE scaffolds. The successful synthesis of AAA-PEAs with different structures was confirmed by nuclear magnetic resonance (NMR) and Fourier transform infrared (FTIR) spectroscopies. Differential scanning calorimetry (DSC) and thermogravimetric analysis (TGA) were employed to study the thermal properties of synthesised materials. The processability of AAA-PEAs was evaluated using dynamic mechanical thermal analysis (DMTA) and complemented by oscillatory rheology, measuring viscosity changes as a function of temperature. Two-dimensional films obtained *via* hot pressing were also used to study the degradation, wettability and mechanical properties of the different AAA-PEAs. 3D printed scaffolds obtained *via* melt-extrusion were morphologically characterised with scanning electronic microscopy (SEM) and micro-computed tomography (micro-CT) and their mechanical behaviour assessed under static compression. *In vitro* biological performance of PEA-based films was studied using human bone marrow derived mesenchymal stem cells (hBM-MSCs) and compared against commercially available PCL.

2. Materials and methods

2.1 Materials

Poly(ε-caprolactone) (PCL, CAPA™ 6500, M_w = 50 000) in the form of 3 mm pellets was obtained from Perstorp Caprolactones (Cheshire, UK) and used as received. Glycine (≥99%), L-alanine (≥99%), *N*-hydroxysuccinimide (NHS) (≥98%), 1,6-hexanediol (≥97%), sebacoyl chloride (≥95%), triethylamine (TEA) (≥99%), *p*-toluenesulfonic acid monohydrate (*p*-TSA) (≥98%) were purchased from Tokyo Chemical Industry (Tokyo, Japan). *O*-(2-Aminopropyl)-*O*-(2-methoxyethyl) polypropylene glycol (Jeffamine® M-600) (jeff) was purchased from Sigma-Aldrich (St. Louis, MO, USA). Toluene (≥99%), ethanol (96%), chloroform (≥99%) and propan-2-ol (≥99%) were supplied by José Manuel Gomes dos Santos Lda (Odivelas, Portugal). Acetonitrile (HPLC-grade) was purchased from CHEM-LAB (Zedelgem, Belgium). Dimethyl sulfoxide (≥99.9%) was purchased from Fisher Scientific (Waltham, Massachusetts, US) and was dried over calcium chloride and distilled prior use. Deuterated dimethyl sulfoxide (DMSO-d_6) and deuterated chloroform ($CDCl_3$) were purchased from Eurisotop (Saint-Aubin, France). Minimum essential medium Eagle and L-ascorbic acid 2-phosphate were purchased from Sigma-Aldrich (St. Gallen SG, Switzerland), TrypLE Express from Gibco (Grand Island, USA), LIVE/DEAD™ Viability Kit and PrestoBlue™ cell viability reagent from Invitrogen™ (Waltham, USA).

2.2 Synthesis of PEAs

2.2.1 Synthesis of the activated diester monomer from sebacoyl chloride. NHS (0.53 mol) and TEA (0.53 mol) were dissolved in 530 mL of acetonitrile inside a reactor vessel, under mechanical stirring (solution 1). In a 250 mL flask, sebacoyl chloride (0.25 mol) was dissolved in 20 mL of acetonitrile, under magnetic stirring (solution 2). Then, solution 2 was added dropwise to solution 1 still under magnetic stirring (Fig. 1(A)). The reactor vessel was placed in an ice bath to ensure that the temperature of the reaction medium was below 25 °C. When the addition was complete, the reaction was allowed to proceed for 2 h at room temperature. Distilled water was added to the reactor, and its content was mechanically stirred for 30 min, to precipitate the product. After, the precipitate was recovered by filtration and transferred to an Erlenmeyer flask and washed twice with distilled water, under stirring. The previous washing step was repeated with ethanol. The product was collected in a glass tray and placed inside a vacuum oven, at 40 °C, until achieving a constant weight. The dried product was recrystallized 4 times in acetonitrile. Then, the product was dried in the vacuum oven, at 40 °C, until constant weight.

White powder. Yield: 80%; ^{1}H NMR (400 MHz, DMSO-d_6 in ppm): 1.30–1.38 (–COO–CH_2–CH_2–$C\underline{H}_2$–$C\underline{H}_2$– signals d and e) 1.63 (–COO–CH_2–$C\underline{H}_2$– c) 2.66 (–COO–$C\underline{H}_2$– signal d) 2.81 (–$C\underline{H}_2$ of NHS, signal a); ^{13}C NMR (400 MHz, DMSO-d_6 in ppm): 24.69 (–COO–CH_2–CH_2–CH_2–$\underline{C}H_2$– signal g) 25.90 (–$\underline{C}H_2$ of NHS, signal a) 28.35 (–COO–CH_2–CH_2–$\underline{C}H_2$ signal f) 28.71 (–COO–CH_2–$\underline{C}H_2$– signal e) 30.64 (–COO–$\underline{C}H_2$– signal d) 169.44 (–$\underline{C}$OO– signal c) 170.71 ($\underline{C}$=O of NHS signal b). FTIR (ATR in cm^{-1}): 2911/2835 (C–H stretch), 1829/1776/1760 (COO–N), 1751 (C=O stretch), 1356 (N–O stretch), 1214 (C–O stretch).

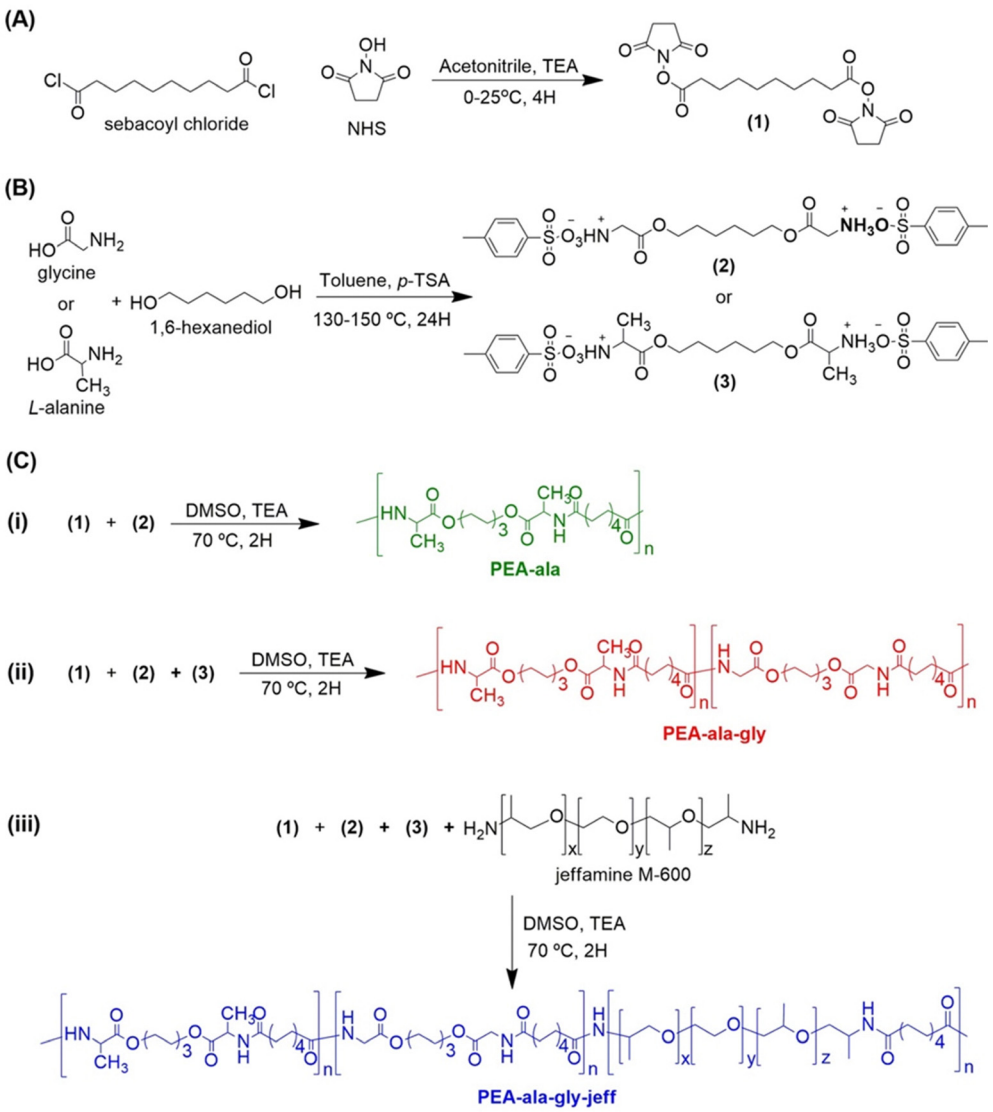

Fig. 1 Synthesis route for activated diester from sebacoyl chloride (A) and bis-α-(L-amino acid)-α,ω-alkylene diesters (B), and for different AAA-PEA by solution polycondensation: (i) L-alanine based PEA, (ii) copolymer of L-alanine and glycine based PEA (PEA-ala–gly) and (ii) copolymer of L-alanine, glycine and jeffamine based PEA (PEA-ala–gly–jeff) (C).

Fig. S1 (ESI†) for ^{1}H NMR spectrum, Fig. S2 (ESI†) for ^{13}C NMR spectrum and Fig. S3 (ESI†) for FTIR spectrum.

2.2.2 Synthesis of bis-α-(L-amino acid)-α,ω-alkylene diester (BAAD) monomers. A suspension of α-amino acid (glycine or L-alanine) (0.24 mol), 1,6-hexanediol (0.12 mol), and *p*-TSA (0.264 mol) in 300 mL of toluene was heated up to 140 °C, in a three-neck round bottom flask equipped with a Dean–Stark apparatus, a condenser with a drying tube, and a mechanical stirrer (Fig. 1(B)). The suspension was heated to reflux until no more water was distilled (18–20 h). The excess of toluene was decanted, and the products were purified by recrystallization.[26] For the glycine-based BAAD (BAAD-gly), the solvent of recrystallization was propan-2-ol. In the case of the L-alanine-based BAAD (BAAD-ala), ethanol was used for recrystallization. The products were recovered by filtration and dried under vacuum, at 40 °C, for 48 h.

BAAD-gly. White powder. Yield: 70%; ^{1}H NMR (400 MHz, DMSO-d_6 in ppm): 1.31 (–COO–CH_2–CH_2–CH_2– signal i), 1.58 (–COO–CH_2–CH_2– signal g), 2.30 (–CH_3 of benzene, signal a), 3.81 (–CH_2–NH_3– signal e), 4.12 (–CH_2–COO– signal h), 7.14 (–CH of benzene, signal b), 7.53 (–CH of benzene, signal b) 8.27 (–NH_3 signal c); ^{13}C NMR (400 MHz, DMSO-d_6 in ppm): 21.25 (–CH_3 of benzene, signal a), 25.25 (–COO–CH_2–CH_2–CH_2– signal i), 28.27 (–COO–CH_2–CH_2– signal g), 39.87 (–CH_2–NH_3– signal e), 65.80 (–CH_2–COO– signal h), 125.98 (–CH of benzene signal b), 128,69 (–CH of benzene signal b), 138.70 (–CH of benzene signal b), 145.22 (–CH of benzene signal b), 168.01 (–COO). FTIR (ATR in cm^{-1}): 3065 (N–H stretch, primary amine salt), 2934 (C–H stretch, aliphatic), 1736 (C═O stretch, ester), 1605 (C–N stretch, primary amine salt), 1509 (C–N stretch, primary amine salt), 1188 (S═O stretch, salt), 1006 (C–O stretch, ester). Fig. S4 (ESI†) for ^{1}H NMR spectrum, Fig. S5 (ESI†) for ^{13}C NMR spectrum and Fig. S6 (ESI†) for FTIR spectrum.

BAAD-ala. White powder. Yield: 80%; ^{1}H NMR (400 MHz, DMSO-d_6 in ppm): 1.32–1.61 (–COO–CH_2–CH_2–CH_2– signals g and i and –NH_3–CH–CH_3 signal d), 2.30 (–CH_3 of benzene, signal a), 4.14 (–CH–NH_3– signal e and –CH_2–COO– signal h), 7.16 (–CH of benzene, signal b), 7.52 (–CH of benzene, signal b), 8.36 (–NH_3 signal c); ^{13}C NMR (400 MHz, DMSO-d_6 in ppm): 16.19 (–NH_3–CH–CH_3 signal d), 21.26 (–CH_3 of benzene, signal a), 25.21 (–COO–CH_2–CH_2–CH_2– signal i), 28.25 (–COO–CH_2– signal g), 38.34 (–CH–NH_3– signal e), 65.97 (–CH_2–COO– signal h), 125.95 (–CH of benzene signal b), 128.64 (–CH of benzene signal b), 138.49 (–CH of benzene signal b), 145.54 (–CH of benzene signal b), 168.00 (–COO). FTIR (ATR in cm^{-1}): 3065 (N–H stretch, primary amine salt), 2934 (C–H stretch, aliphatic), 1736 (C═O stretch, ester), 1605 (C–N stretch, primary amine salt), 1509 (C–N stretch, primary amine salt), 1188 (S═O stretch, salt), 1006 (C–O stretch, ester). Fig. S4 (ESI†) for ^{1}H NMR spectrum, Fig. S5 (ESI†) for ^{13}C NMR spectrum Fig. S6 (ESI†) for FTIR spectrum.

2.2.3 Synthesis of the α-amino acid based poly(ester amide)s (AAA-PEAs). Three AAA-PEAs with different chemical structures were synthesized *via* solution polycondensation.[27] In a round bottom flask, the diamine monomers (BAAD-ala or BAAD-ala and BAAD-gly or BAAD-ala, BAAD-gly and jeff) and TEA were dissolved in dry DMSO, at 70 °C, under mechanical stirring. Upon complete dissolution, the activated diester of sebacoyl chloride was added, and the reaction was allowed to proceed for 2 h (Fig. 1(C)). Afterwards, the reaction medium was diluted with chloroform and placed in a separatory funnel for washing with distilled water. The obtained organic phase was separated from the aqueous phase, and the former was placed in a Teflon plate to allow the evaporation of the organic solvent. The obtained product was purified using a Soxhlet extraction in ethyl acetate for 72 h. The purified AAA-PEA was dried in a vacuum oven, at 40 °C, for 48 h to obtain transparent films. The yield was always very consistent with small variations (40% to 50%) between runs. The quantity of reactants used in the synthesis of each AAA-PEA is reported in Table S1 (ESI†).

2.3 Characterization of activated diester, BAADs and AAA-PEAs

2.3.1 Chemical structure of the activated diester, BAADs and AAA-PEAs. The chemical structure of BAADs, activated diester and AAA-PEAs was characterized by proton and carbon nuclear magnetic resonance (^{1}H NMR and ^{13}C NMR) and by Fourier transform infrared (FTIR) spectroscopies. ^{1}H NMR spectra were obtained in DMSO-d_6 for BAADs and activated ester and in $CDCl_3$ for AAA-PEAs. The analysis was carried out at 25 °C on a Bruker Avance III 400 MHz spectrometer using a 5 mm TIX triple resonance detection probe. Tetramethylsilane was used as the internal standard. FTIR analysis was carried out with a Cary 630 FTIR spectrometer. Data collection was performed with 4 cm^{-1} spectral resolution and 64 accumulations in a 750 and 4000 cm^{-1} wavenumber range.

2.3.2 Molecular weight distribution. The number-average (M_n), weight-average (M_w) molecular weight and polydispersity ($Đ = M_w/M_n$) of the AAA-PEAs were determined by size-exclusion chromatography (SEC) using a Viscotek (Viscotek TDAmax) equipment, equipped with a refractive index (RI) detector. The column set consisted of a PLgel MiniMIX-E 3 μm guard column followed by one Viscotek T4000 column, one Viscotek D2000 column, and one Styragel HR column (5 μm). A dual piston pump was set with a flow rate of 1 mL min^{-1}. The eluent (DMF with 0.03% w/v LiBr) was previously filtered through a 0.2 μm filter. The system was also equipped with an online degasser. The tests were carried out at 60 °C using an Elder CH-150 heater. Before the injection (100 μL), the samples were filtered through a polytetrafluoroethylene (PTFE) membrane with 0.2 μm pore. The system was calibrated with narrow PMMA standards. M_w and $Đ$ of the synthesized polymers were determined by conventional calibration using the OmniSEC software version: 4.6.1.354.

2.3.3 Thermal properties. The thermal behavior of the AAA-PEAs, PCL and respective scaffolds was studied by differential scanning calorimetry (DSC) in a Netzsch DSC 204 F1 Phoenix model. The heat flow capacity and temperature sensitivity were calibrated at a 5 K min^{-1} heating rate using

adamantane, indium, tin, bismuth, and zinc as standards. The samples were analyzed in closed aluminum pans with pierced aluminium lids. Sample weights ranging from 8 to 11 mg were used. A heating rate of 5 K min^{-1} and a dry nitrogen purge flow of 50 mL min^{-1} were used in all measurements. The temperature was initially equilibrated at −95 °C. Then, the samples were heated from −95 to 190 °C at 5 K min^{-1}, followed by a cooling run to −95 °C at 5 K min^{-1}, and finally by a second heating run from −95 to 260 °C at 5 K min^{-1}. The thermal stability of AAA-PEAs and PCL was evaluated by thermogravimetric analysis (TGA) in a Netzsch TG 209 F1 Libra equipment (thermobalance sensitivity: 0.1 μg), from 30 °C to 600 °C, at a heating rate of 10 K min^{-1}, using open alumina crucibles and a dry nitrogen purge flow of 50 mL min^{-1}. Additionally, the AAA-PEAs and PCL were subjected to an isothermal TGA, at 100 °C, for 10 h. Sample weights ranging from 9 to 11 mg were used. The equipment was previously calibrated at 10 K min^{-1} heating rate by using the c-DTA signal for indium, tin, bismuth, zinc, aluminium, and gold as melting standards.

2.4 Preparation and characterization AAA-PEA films

The AAA-PEAs and PCL films were prepared by hot pressing in a laboratory hydraulic press (CARVER®), at 100 °C, and 0.1 metric tons for 15 min. Afterwards, the films were allowed to cool down at room temperature until complete solidification. Cardboard molds were used to ensure the fabrication of films with homogeneous and constant thickness (≈0.3 mm).

2.4.1 Thermomechanical properties. Dynamic mechanical thermal analysis (DMTA) was performed on samples of AAA-PEAs and PCL films with dimensions of 12.0 mm × 4.0 mm × 0.4 mm. The analysis was performed in tension mode using a Netzsch DMA 242D equipment. The tests were carried out from −50 °C to 40 °C for PEA-ala and PEA-ala–gly and from −100 to 40 °C for PEA-ala–gly–jeff and PCL, in multifrequency mode (1, 2, 5, 10 Hz), with a heating rate of 5 K min^{-1}. The T_g of the samples was determined from the maximum of the tan δ *vs.* T curve, at 1 Hz.

2.4.2 Nanoindentation tests. Nanoindentation tests were carried out on polymeric films of PEA-ala, PEA-ala–gly, PEA-ala–gly–jeff and PCL. The measurements were performed in 1 mN to 5 mN load range using a Nanotest Platform (Micromaterials, UK) with a diamond pyramid-shaped Berkovich-type indenter tip. The tests were performed in a load-controlled mode using trapezoidal functions with a hold period of 20 s at the maximum load and a loading–unloading rate of 300 μN s^{-1}. The load–depth curves were recorded, and the hardness values were evaluated using the Oliver and Pharr method. Specifically, the hardness (H) was determined as follows eqn (1):

$$H = P_{max}/A_c \quad (1)$$

with P_{max} and A_c being the applied peak load and the projected contact area at the specified load, respectively. The determination of A_c was clearly made according to the penetration depth and the geometry of the employed tip.

2.4.3 Water contact angle measurements. Water contact angle measurements were performed on AAA-PEAs and PCL films using a Drop Shape Analyzer DSA 100 (KRUSS, USA). Distilled water was dropped on the surface of the films at various points and the contact angle was evaluated. The CF04 camera system recorded the process of the droplet dropping on the film. The baseline for the contact angle of a sessile drop was determined at the liquid–solid interphase. The contact angles were evaluated using the ellipse method for the extraction of the drop profile, and reported as mean value ± standard deviation.[23]

2.4.4 *In vitro* degradation. *In vitro* enzymatic and hydrolytic degradation tests were performed in PBS (pH = 7.4, 0.01 M) with and without α-chymotrypsin enzyme (0.4 mg mL^{-1}), respectively. Films of AAA-PEAs and PCL were cut into smaller specimens, weighing approximately 50 mg, and immersed in 2.5 mL of either hydrolytic (PBS) or enzymatic solution (PBS and enzyme) and incubated for 4 weeks at 37 °C. The enzymatic medium was renewed every week to avoid loss of enzymatic activity. At predetermined times (1, 2, 3 and 4 weeks) the samples were removed from degradation medium, washed thoroughly with water, and dried under vacuum to constant weight. The degree of degradation was estimated from the weight loss, according to eqn (2).

$$\text{Weight loss}\,(\%) = \frac{W_0 - W_t}{W_0} \times 100 \quad (2)$$

where W_0 is the initial weight of the dry samples before immersion, and W_t is the weight of the dry samples, after incubation for t week(s). Five technical replicates were performed.

2.5 *In vitro* biological tests

2.5.1 Cell culture. Primary human bone marrow-derived mesenchymal stem cells (hBM-MSC) were derived from a single donor (male, 81 years old) and isolated as described by Strassburg *et al.*[28] following approval from the National Research Ethics Committee (reference: 10/H1013/27) and fully informed written consent from the patient. hBM-MSCs were cultured in Minimum Essential Medium Eagle (Alpha Modification, with sodium bicarbonate) supplemented with 10% fetal calf serum, antibiotics (100 U mL^{-1} penicillin, 100 mg mL^{-1} streptomycin, 0.25 μg amphotericin), 1% glutamax and 10 μM L-ascorbic acid 2-phosphate (referred to as hBM-MSCs CCM). Cells were maintained at 37 °C and 5% CO_2 and media changed every 2–3 days. Cells were subcultured at *ca.* 70–80% confluence and dissociated with TrypLE Express, before reseeding. hBM-MSCs between passage 4–7 were used for subsequent experiments.

2.5.2 Cell culture on AAA-PEAs and PCL films. In preparation for biological studies described below, AAA-PEAs and PCL films were cut into disc-shaped specimens (12 mm diameter) using a punch tool, placed inside a 24-well plate, covered with a 70% ethanol solution for 5 minutes and then washed twice with PBS. To complete the sterilization process, the films were transferred to a new 24-well plate, placed inside a biosafety cabinet and irradiated with UV light for 4 h before adding cell culture medium (hBM-MSCs CCM). Prior to cell seeding, the culture medium was removed, and the films were washed with

PBS twice. Finally, 60 000 cells per cm^2 and 40 000 cells per cm^2 were seeded on top of polymeric films for cell viability and cell morphology studies, respectively, and incubated at 37 °C and 5% CO_2 for a maximum of 28 days. The culture medium was refreshed every 2–3 days.

2.5.3 Cell viability. Cell viability was evaluated at day 7 of *in vitro* culture using a LIVE/DEAD™ Viability/Cytotoxicity Kit. Cell-seeded films of PCL and AAA-PEAs were first incubated with 2 μM calcein AM and 4 μM ethidium homodimer-1 (EthD-1) in PBS for 30 minutes at 37 °C and 5% CO_2. Afterwards, the films were washed with PBS and imaged using a Leica TCS SP8 (Leica Microsystems, Germany) at excitation/emissions wavelengths of 495 nm/500–540 nm and 642 nm/600–670 nm, respectively to each stain. Obtained images were used to determine the percentage of cell viability following the manufacturers protocol. LIVE/DEAD™ assays were carried out in triplicate and plastic tissue culture plate was used as 2D positive control.

2.5.4 Metabolic activity. The metabolic activity of hBM-MSCs in contact with formulated materials was determined by PrestoBlue™ assay using both direct and indirect methods. The latter was employed due to difficulties in finding adherent cells on the surface of jeffamine-based PEA films.

Direct contact tests were performed at day 1, 3, 7, 14, 21 and 28 post-seeding with hBM-MSCs. AAA-PEAs and PCL films were washed twice with PBS and incubated with 10% (v/v) of PrestoBlue™ solution for 4 hours at 37 °C and 5% CO_2. Absorbance was recorded at 590 nm using a Spark® Multimode Microplate Reader (Tecan, Switzerland) in triplicate (3 films per material and time point).

For indirect contact tests, sterilized AAA-PEAs and PCL films were placed in a 24-well culture plate and incubated at 37 °C and 5% CO_2 with 1 mL of hBM-MSCs CCM for 24 hours. hBM-MSCs were seeded at 60 000 cells per cm^2 in a separate 24 well plate with 1 mL of hBM-MSCs CCM. After 24 h the cell culture media of hBM-MSCs was removed and replaced with the eluate from PCL and AAA-PEA films and incubated for 48 h at 37 °C and 5% CO_2. PrestoBlue™ assay was then performed in triplicate (3 films per material and time point) using the same protocol reported for the indirect contact test.

2.5.5 Cell morphology. After 7 days of incubation, AAA-PEAs and PCL films and 2D controls, were washed twice with PBS and fixed with 4% (w/v) of paraformaldehyde. Next, samples were washed twice, permeabilized and blocked with 0.1% (w/v) Triton X-100 in 1% (w/v) BSA in PBS for 30 minutes. Films were then incubated in ActinRed™ 555 (2 drops per mL) for one hour, washed twice with PBS, then counterstained with 5 μg mL^{-1} Hoechst 33342 in PBS for 10 minutes. Stained films were washed a further two times with PBS to remove excess stain, then imaged using a Leica TCS SP8 (Leica Microsystems, Germany) at excitation/emissions wavelengths of 405 nm/410–500 nm and 540 nm/530–600 nm, respectively to each stain. Depth projections were created using ImageJ software.

2.6 Scaffold fabrication and characterization

An extrusion-based 3D printing system (3D Discovery, regenHU, Switzerland) equipped with a screw-driven printing head and a 330 μm nozzle was employed in the fabrication of both PCL and AAA-PEAs scaffolds. Rectangular prisms measuring 30 mm (length) × 30 mm (width) × 2 mm (height) were initially designed (Fig. 1) using BioCAD software (regenHU, Switzerland) and subsequently printed employing an optimized set of parameters (Table S2, ESI†). A regular internal pore geometry (quadrangular) was selected to investigate the shape fidelity of printed constructs. This geometry was defined by keeping a constant filament distance (FD) of 730 μm and alternating the deposition angle between 0° and 90° in adjacent layers (Fig. 2). These parameters were defined based on our group's previous work on screw-assisted printing of PCL scaffolds,[29] with minor adjustments to the deposition velocity (DV) and liquefier temperature (LT) to ensure the extrusion of continuous filaments with RW values comparable to the internal diameter of the nozzle used (*i.e.*, 330 μm). Scaffolds with 30 mm (length) × 30 mm (width) × 4 mm (height) were also printed for mechanical testing. The obtained scaffolds were then cut into smaller specimens and used for further analyses.

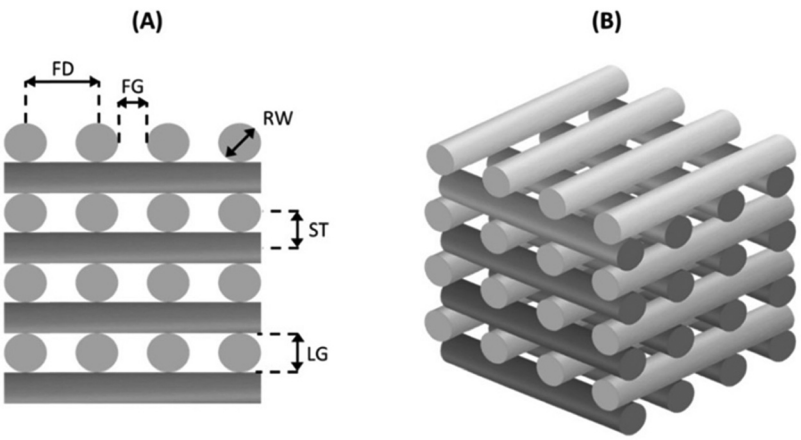

Fig. 2 Schematic representation of the side view of the scaffold with 0/90° deposition angle showing the road width (RW), filament distance (FD), filament gap (FG) layer gap (LG) and the slice thickness (ST) (A) and 3D CAD model (B).

2.6.1 Scanning electron microscopy. The morphology of the 3D printed PCL and AAA-PEAs scaffolds was analyzed by scanning electron microscopy (SEM) (TESCAN VEGA3 SEM, Czech Republic). After gold-sputtering (5 nm) of the AAA-PEAs and PCL scaffolds (Quorum Q150T, Quorum Technologies, Sussex, UK), top and cross-sectional SEM micrographs were obtained under high vacuum conditions at a voltage of 10 kV. ImageJ software (National Institute of Health, Bethesda, MD, USA) was then used to evaluate the structural integrity of the scaffolds and the agreement between theoretical (pre-defined in the BioCAD) and experimental values of RW and FG.

2.6.2 Micro-computed tomography. Micro-computed tomography (micro-CT) analysis of the 3D printed AAA-PEAs and PCL scaffolds was performed with a rotation pitch of 0.9° over an angle of 180°, using the SkyScan 1072 system (Aartselaar, Belgium). Different software programs (SkyScan software package, ImageJ software – NIH, Bethesda, MD, USA, and Mimics software – Materialise, Leuven, Belgium) were used to reconstruct the 3D printed scaffolds and thus to evaluate the porosity values, surface area-to-volume ratio and interconnectivity.

2.6.3 Mechanical testing. Mechanical compression tests were performed on 3D printed AAA-PEAs and PCL scaffolds using block-shaped specimens (length – l_0 of 4.0 mm, width – w_0 of 4.0 mm, height – h_0 of 4.0 mm). The specimens were immersed in PBS for 24 hours at 37 °C before testing at a rate of 1 mm min^{-1} up to a strain of 50%, using an INSTRON 5566 machine.

Considering the measured force (F) and the initial cross-sectional area of the specimen ($A_0 = l_0 \cdot w_0$), the engineering stress (σ) was calculated as follows eqn (3):

$$\sigma = F/A_0 \quad (3)$$

The engineering strain (ε) was evaluated as the ratio between the initial height (h_0) and the height variation (Δh) of the specimen (eqn (4)):

$$\varepsilon = \Delta h/h_0 \quad (4)$$

The compressive Young's modulus (E) was calculated as the slope of the initial linear region of the stress–strain curve.

2.7 Statistical analysis

Statistical analyses were performed using one-way analysis (ANOVA) followed by Tukey's multiple comparison tests; statistical differences were set for $p < 0.0001$, $p < 0.001$, $p < 0.01$, and $p < 0.1$.

3. Results and discussion

3.1 Synthesis and characterization of AAA-PEAs

3.1.1 Chemical characterization. The synthesis of AAA-PEAs was conducted through a three-stage active solution polycondensation process (Fig. 1) comprising: (i) synthesis of the activated diester of sebacoyl chloride (Fig. 1(A)); (ii) synthesis of the BAADs (Fig. 1(B)); and (iii) synthesis of the AAA-PEAs (Fig. 1(C)). The activated diester was successfully synthesized from the reaction of sebacoyl chloride and NHS (Fig. S1–S3 for the ^{1}H NMR, ^{13}C NMR and FTIR, respectively, ESI†). Pre-activated diacids are normally used in polymerization reactions to enable polymerization at low temperature (70 °C), yielding side-product free polycondensates and predictable degradation products.[30] The BAADs were synthesized through the esterification reaction of glycine or L-alanine with 1,6-hexanediol, in the presence of *p*-TSA.[27] The chemical structure of the BAADs (BAAD-gly and BAAD-ala, respectively) was confirmed by ^{1}H NMR, ^{13}C NMR and FTIR spectroscopies (Fig. S4–S6, ESI†).

High molecular weight is a desirable feature in polymeric materials for melt-extrusion 3D printing, and various groups have previously reported the successful formulation of AAA-PEAs with M_w in the range of 30 kDa to 60 kDa.[31–35] However, only recently Ansari *et al.*[24] managed to synthesize glycine-based PEAs *via* active solution polycondensation with suitable M_w (50 kDa) under 2 hours (50 minutes) of reaction time. Like Ansari *et al.* we have decided to start investigating the molecular weight evolution of our reactions over time to determine the feasibility of our approach to generate high molecular weight PEAs with short reaction times. The results (Fig. 3) show that the PEA-ala reached the maximum molecular weight of 72 kDa, after 10 minutes, while the PEA-ala–gly and PEA-ala–gly–jeff attained the maximum molecular weight of 82 kDa and 77 kDa, respectively, after 20 minutes of reaction. The polydispersity ($Đ$) values of were between 1.3 and 1.5.

Regarding M_w, a statistically significant difference was observed between PEA-ala and the other AAA-PEAs at the plateau. The molecular weight variations may stem from using SEC with conventional calibration, as this method estimates M_w based on the comparison of the hydrodynamic volume of the polymers with polymer standards (in this case, PMMA standards), and structural differences among the AAA-PEAs could affect the results. Additionally, the step-growth polymerization process is sensitive to reactant stoichiometry, and minor reactant weighing discrepancies might have caused fluctuations in M_w. Regarding $Đ$, no statistically significant differences were noted among the PEAs at different time points.

The FTIR spectra (Fig. S7, ESI†) present the main bands corresponding to the ester and amide bonds of AAA-PEAs. At 1734 cm^{-1}, the band associated with the stretching vibration of the –C═O_{ester} is observed. It is also possible to identify the bands corresponding to the stretching vibration of –NH_{amide} and –C═O_{amide}, at *ca.* 3310 cm^{-1} and 1638 cm^{-1}, respectively. The bands between 1520–1540 cm^{-1} are assigned to the bending vibration and stretching vibration of the –NH_{amide} and C–N_{amide}.

Fig. 4 shows the ^{1}H NMR spectra of the AAA-PEAs. In all spectra, it is possible to see the resonances of the –CH_2 protons next to the amide linkage and ester linkage at 2.1 ppm (d) and 4.1 ppm (a), respectively. Between 1.2 and 1.6 ppm, resonate the protons belonging to the central –CH_2 protons (b, c, e, f, g and respective ′ and ″) of both sebacate and 1,6-hexanediol units, and also the protons ascribed to the –CH_3 groups (i) of L-alanine. The resonance of the amide proton (l) is clearly visible at 6.2 ppm for all AAA-PEAs. Additionally, in

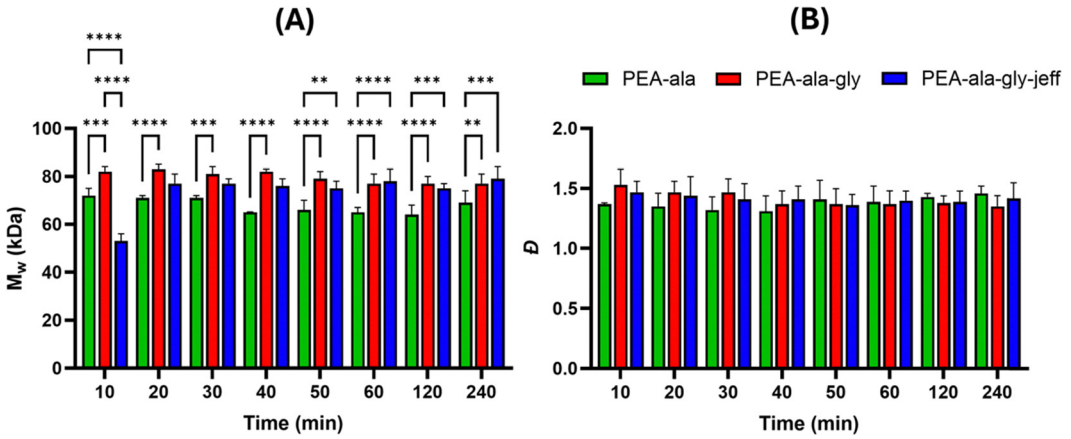

Fig. 3 Evolution of molecular weight (M_w) (A) and polydispersity ($Đ$) (B) as a function of time for AAA-PEAs made *via* active solution polycondensation. Data are reported as mean value and error bar represents the standard deviation. Statistical analysis was performed using two-way ANOVA followed by Tukey's: (****) $p < 0.0001$, (***) $p < 0.001$, and (**) $p < 0.01$.

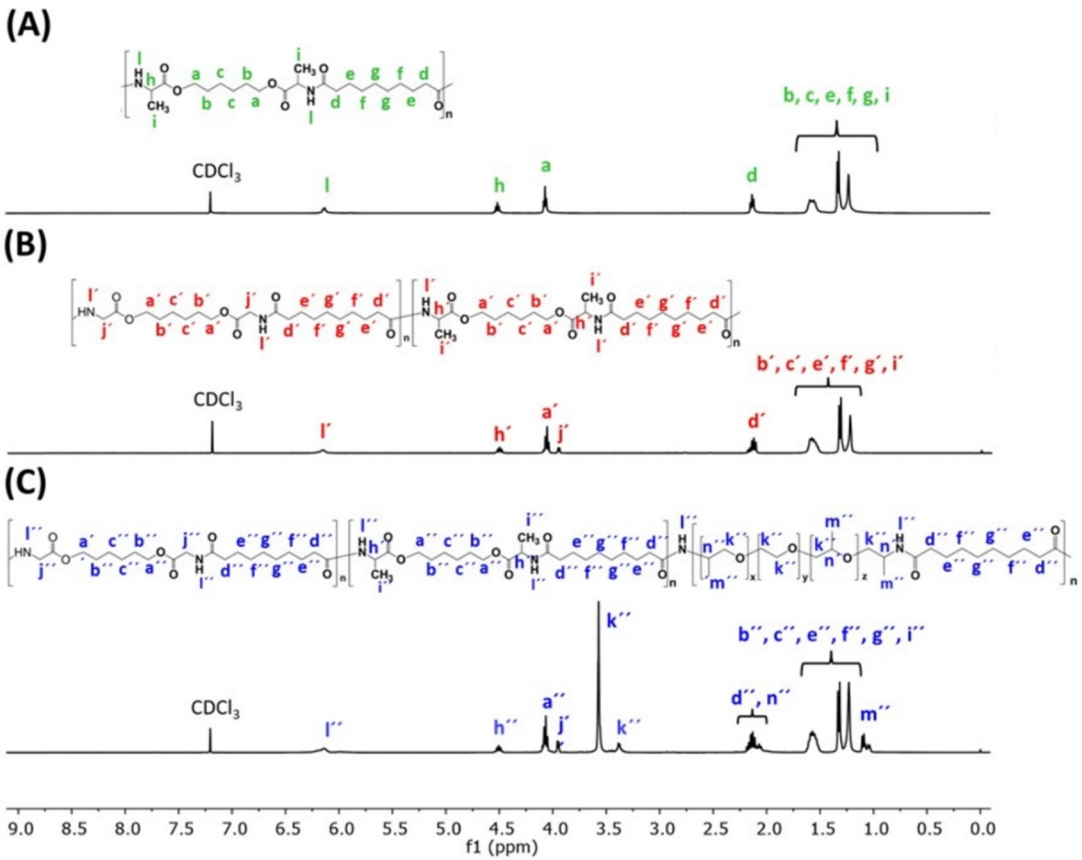

Fig. 4 ^{1}H NMR spectra of PEA-ala (A) and PEA-gly-ala (B) and PEA-ala–gly–jeff (C).

the AAA-PEAs containing glycine, it is possible to identify its –CH_2 protons (j′ and j″) at 3.9 ppm. In AAA-PEAs containing jeff units, it is possible to see the signals at 3.2–3.8 ppm (k″) assigned to the –CH and –CH_2 protons and the signals at 1.0–1.2 ppm (m″) corresponding to the –CH_3 protons of jeff.

The molar ratio of each monomer (BAAD-ala; BAAD-gly and jeff) in the copolymers of PEA-gly-ala and PEA-ala–gly–jeff was calculated from the integration areas of the ^{1}H NMR peaks corresponding to the protons of glycine, L-alanine and jeff. For the L-alanine block, the integration areas of the "(h′ or h″)" protons were considered while for the glycine groups, the peak of the "(j′ or j″)" protons was selected for integration. The same was done to calculate the molar fraction of jeff, where the area of "(m″)" protons was considered. The in feed and the actual

molar ratios of the different monomers in the copolymers are presented in Table S3 (ESI†). For both copolymers, the molar ratios of the individual monomers were within the expected values, indicating that all monomers had similar reactivities with the activated diester of sebacoyl chloride. Further insights into the chemical structure of AAA-PEAs were provided by ^{13}C NMR spectroscopy (Fig. S8, ESI†). The data provided by FTIR and ^{1}H NMR and ^{13}C NMR spectroscopies are in full agreement with the proposed chemical structure of the AAA-PEAs, suggesting a successful synthesis of the polymers.

3.1.2 Thermal analysis. DSC and TGA were employed to study the thermal properties of formulated AAA-PEAs and gain insights into their processing *via* melt-extrusion 3D printing.

Thermogravimetric analyses (Fig. 5(A) and (B)) show clear differences in terms of stability and thermal degradation profile between AAA-PEAs and PCL. As evidenced by DTG curves, AAA-PEAs degrade in two or three stages, commonly attributed to the degradation of the ester (T_{p1} = 369.3–371.8 °C) and amide linkages (T_{p2} = 412.4–421.4 °C and T_{p3} = 458.8–420.0 °C). PCL instead present a single stage related to the degradation of its ester linkages at 407.9 ± 1.6 °C.[25,36,37] The $T_{5\%}$ (Table S4, ESI†), which is the temperature at which the samples lose 5% of their initial weight, is similar for all the AAA-PEAs (between 335 °C to 340 °C), indicating a similar thermal stability profile, while PCL showed slightly higher value of $T_{5\%}$ (375 °C). A non-volatile char residue is observed for the AAA-PEAs (Table S4, ESI†), which can be attributed to the occurrence of crosslinking and/or cyclization reactions during the thermal degradation of these polymers.[25]

The thermal properties of AAA-PEAs and PCL, below the degradation temperature, were evaluated by DSC (Fig. 5(C)–(F)). In the first heating run, the AAA-PEAs show an endothermal

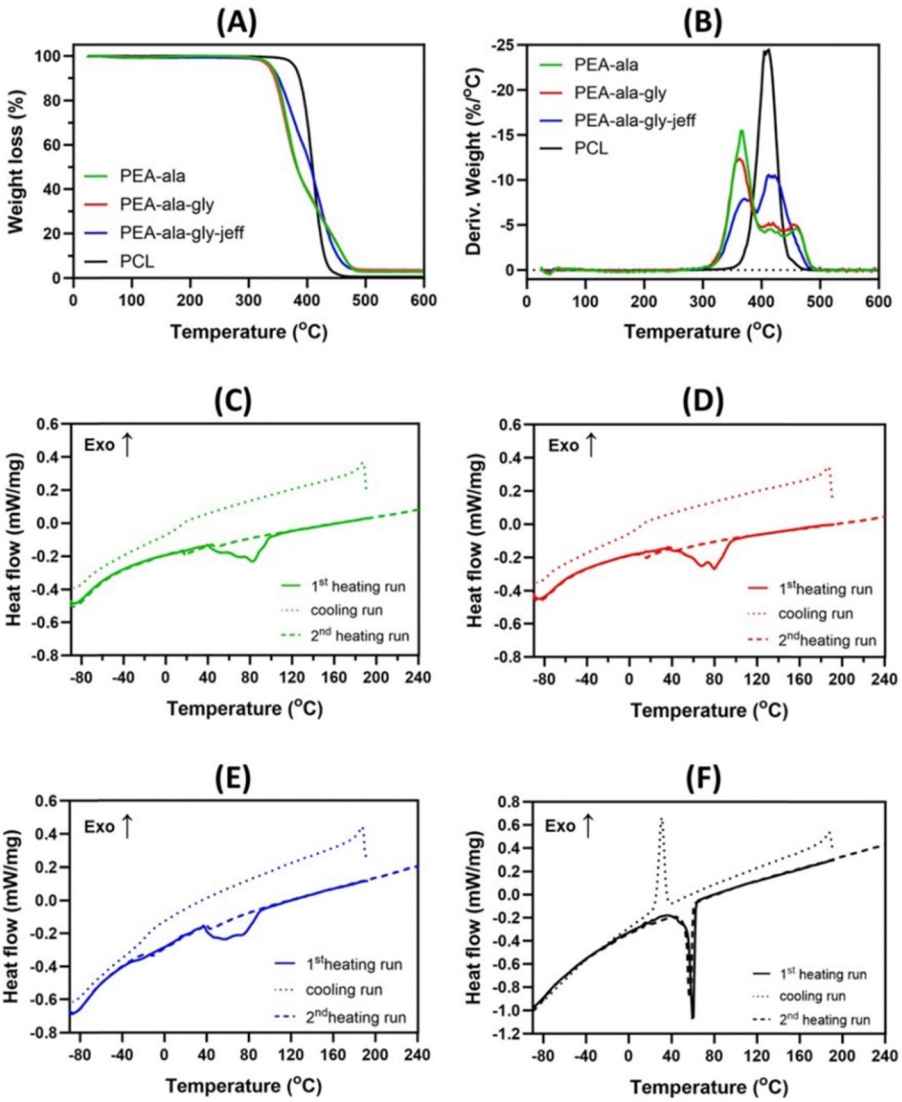

Fig. 5 Thermogravimetric analysis of AAA-PEAs and PCL at 10 K min^{-1}: TG (A); DTG (B). DSCs traces of the PEA-ala (C), PEA-ala–gly (D), PEA-ala–gly–jeff (E) and PCL (F): the sequence of three DSC runs carried out with the samples is as follows: a first heating run at 5 K min^{-1}, a cooling run at 5 K min^{-1} after keeping the sample in the molten state for 5 min, and a reheating run at 5 K min^{-1}.

event that is consistent with a melting, indicating that after synthesis and purification, the polymers present a semi-crystalline nature. The melting transition is broad, suggesting the presence of crystalline structures with different organizations within the samples. In the cooling run and in the subsequent heating run, the only thermal event that is observed is a glass transition, indicating that the AAA-PEAs are not able to crystallize from the melt, under the conditions used in the analysis. This result may be a consequence of the presence of the methyl side groups of L-alanine, preventing a close chain packing and crystallization.[37] The glass transition temperature (T_g) of PEA-ala–gly–jeff was much lower ($T_g = -13$ °C) compared to the other AAA-PEAs (12 °C < T_g < 18 °C). This result can be ascribed to the presence of flexible ether linkages in the jeffamine which facilitate free rotation. Our data agrees with literature, where T_g values for L-alanine and glycine-based PEAs have been reported in the range of 0–25 °C.[24,36] PCL shows a different behavior compared to AAA-PEA but in line with previous studies.[25] In both the first and second heating runs, a single endothermic peak is visible at about 56 °C, corresponding to the melting of the polymer and indicating a semi-crystalline behavior. During cooling, a well-defined exothermic peak is observed at about 30 °C, corresponding to a crystallization process.

3.2 Characterization of AAA-PEA films

3.2.1 Thermomechanical properties. The thermomechanical properties of the films were analysed by DMTA, in multifrequency mode, using a heating rate of 5 °C min^{-1}. Fig. 6(A)–(D) presents the log E' and tan δ curves of the films at the frequency of 1 Hz. The T_g of the films was determined from the maximum of tan δ, at 1 Hz. The tan δ curves of the films in multifrequency mode are presented in ESI† (Fig. S9).

In the E' profile (Fig. 6(A) and (B)), for the AAA-PEAs films, two regions can be distinguished: (1) the glassy region from −100 °C to *ca.* −45 °C for the PEA-ala–gly–jeff films, and from −50 °C to −10 °C for the PEA-ala and PEA-ala–gly films, in which the materials behave as stiff materials; (2) the glass transition zone, in which a decrease in the E' values can be observed. In comparison, this decrease takes place in a narrower temperature range for the AAA-PEA films suggesting a lower degree of crystallinity, which corroborates the DSC results.

In Fig. 6(C) and (D) it is possible to observe that AAA-PEAs films have a narrower tan δ profile compared to the PCL films. This result could also be due to the higher crystallinity of the PCL films. As previously reported,[25] in materials with higher crystallinity, the amorphous domains have more difficulty starting their motion due to their confinement in the crystalline domains, resulting in wider tan δ peaks. AAA-PEAs, in particular those with jeffamine, exhibit higher tan δ peaks denoting a better capacity to absorb and dissipate energy (damping effect) compared to PCL materials. Table S5 (ESI†) summarizes the values of E', at 37 °C, and the T_g values of the films.

The results show a higher E' value for PEA-ala and PEA-ala–gly films compared to PEA-ala–gly–jeff films, indicating a higher polymeric chain mobility and lower stiffness associated with the presence of ether linkages in the structure of the latter. Differences in mechanical properties, particularly substrate stiffness, have been extensively studied for their ability to direct

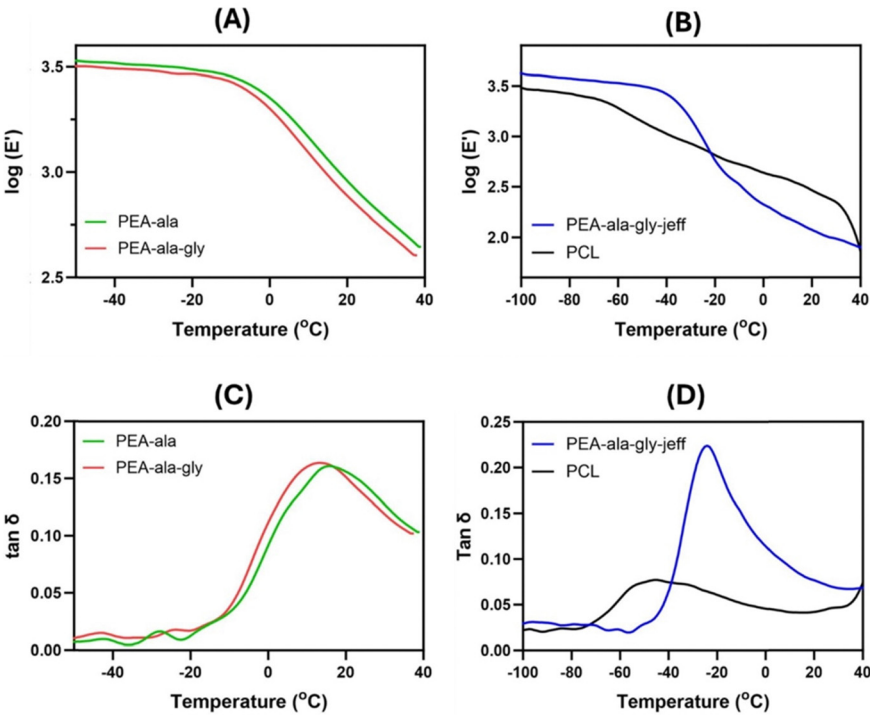

Fig. 6 DMTA traces of the AAA-PEAs and PCL films log(E') *vs.* temperature (A) and (B), and tan δ *vs.* temperature (C) and (D).

cell behavior by activating various mechanotransduction pathways.[38–40] These pathways, which include mechano-regulated ion channels[41] and focal adhesion complexes in the plasma membrane, influence transcriptional and proteomic regulation, morphology and lineage commitment. Although the biological results did not reveal significant differences in cellular morphology (see Section 3.2.4), formulating AAA-PEAs with varying degrees of stiffness remains relevant and warrants further investigation to explore their impact on other cellular processes, such as stem cell differentiation. E' values for PCL at 37 °C are not reported due to the initial melting of the polymer as confirmed by an abrupt change in the E' profile just after the glass transition zone. No significant changes were detected between pristine and processed AAA-PEAs (*i.e.* films) in terms of T_g suggesting that hot pressing does not affect the intrinsic thermal properties of the AAA-PEAs.

3.2.2 Surface properties. The wettability and hydrophilicity of the different materials was evaluated by water contact angle (WCA) measurements (Fig. 7(A)) performed on the surface of 2D films. Obtained results show a higher WCA value for PCL (*ca.* 88.7°) compared to PEA-ala (*ca.* 79.3°), likely related to the presence of amide bonds in the structure of the AAA-PEAs. The introduction of glycine in the PEAs formulation (PEA-ala–gly) resulted in a further decrease of WCA value (*ca.* 69.0°) probably due to the decrease in the amount of hydrophobic pendant –CH_3 groups in the structure.[42] The presence of ether groups in the structure of AAA-PEAs led to a significant increase in hydrophilicity, demonstrated by the smallest WCA measured on PEA-ala–gly–jeff films (*ca.* 35.8°). Surface properties including wettability, are known to play a key role in a multitude of cellular processes, from initial cell adhesion to differentiation.[43] Our work opens the possibility of controlling such processes – at least partly – by synthesizing AAA-PEAs with different structures and degrees of hydrophilicity.

Nanoindentation measurements were carried out to map the surface mechanical properties and evaluate the microstructural characteristics of the bulk materials that may influence cell–matrix interactions and determine cell adhesion, proliferation, differentiation, and even phenotype.[44–46] Fig. 7(B) shows the results of nanoindentation tests on PEA-ala, PEA-ala–gly, PEA-ala–gly–jeff, and PCL films in terms of hardness as a function of applied load.

The measurements on the PCL films showed hardness values between 0.49 GPa and 0.29 GPa in the tested load range. These values were higher than those determined for PEA-ala (from 0.28 GPa to 0.16 GPa), PEA-ala–gly (from 0.39 GPa to 0.24 GPa), and PEA-ala–gly–jeff (from 0.21 GPa to 0.12 GPa) films. The lowest hardness values were obtained for PEA-ala–gly–jeff films, and the differences observed between the different groups were statistically significant at each load point. These differences in hardness between the films prepared from the different AAA-PEAs indicate that their mechanical properties can be easily altered by changing the chemical structure of the PEAs. PEA-ala–gly–jeff leads to films with a lower hardness due to the presence of ether groups in its structure, which allow a higher mobility of the polymer chains. The films made from PEA-ala–gly have a higher hardness than those made from PEA-ala, possibly due to the greater compaction of the polymer chains in PEA-ala–gly, which is due to the absence of a side group in glycine.

3.2.3 *In vitro* hydrolytic and enzymatic degradation. Controlled degradation is essential to ensure a correct transfer of loads between the engineered biomaterial or scaffold and the newly formed tissue *in vivo*. Accelerated or delayed degradation kinetics may result in premature failure of the scaffold or prevent tissue ingrowth, respectively. In this work, we studied the *in vitro* degradation of AAA-PEAs films under hydrolytic and enzymatic conditions to inform scaffold design in future TE

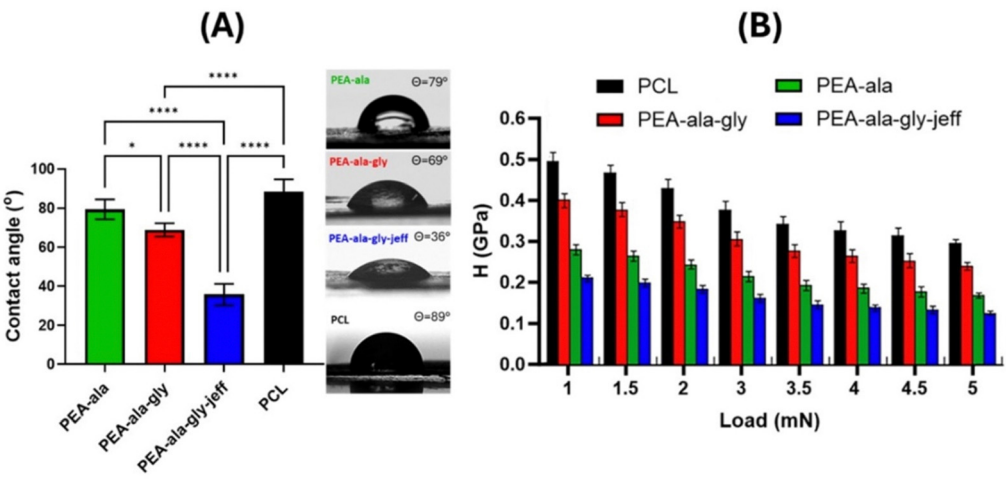

Fig. 7 Average WCA values for films of PCL and AAA-PEAs (left) and image of the water droplet on the surfaces of PEA-ala, PEA-ala–gly, PEA-ala–gly–jeff and PCL films (right). Data are reported as mean value and error bar represents the standard deviation. Statistical analysis was performed using ANOVA followed by Tukey's: (****) $p < 0.0001$ and (*) $p < 0.1$ (A). Results obtained from nanoindentation tests on the different films (PEA-ala, PEA-ala–gly, PEA-ala–gly–jeff, and PCL): hardness as a function of the applied load (1–5 mN). Data are reported as mean value and error bar represents the standard deviation. The different groups were statistically significant ($p < 0.0001$) at each load point (B).

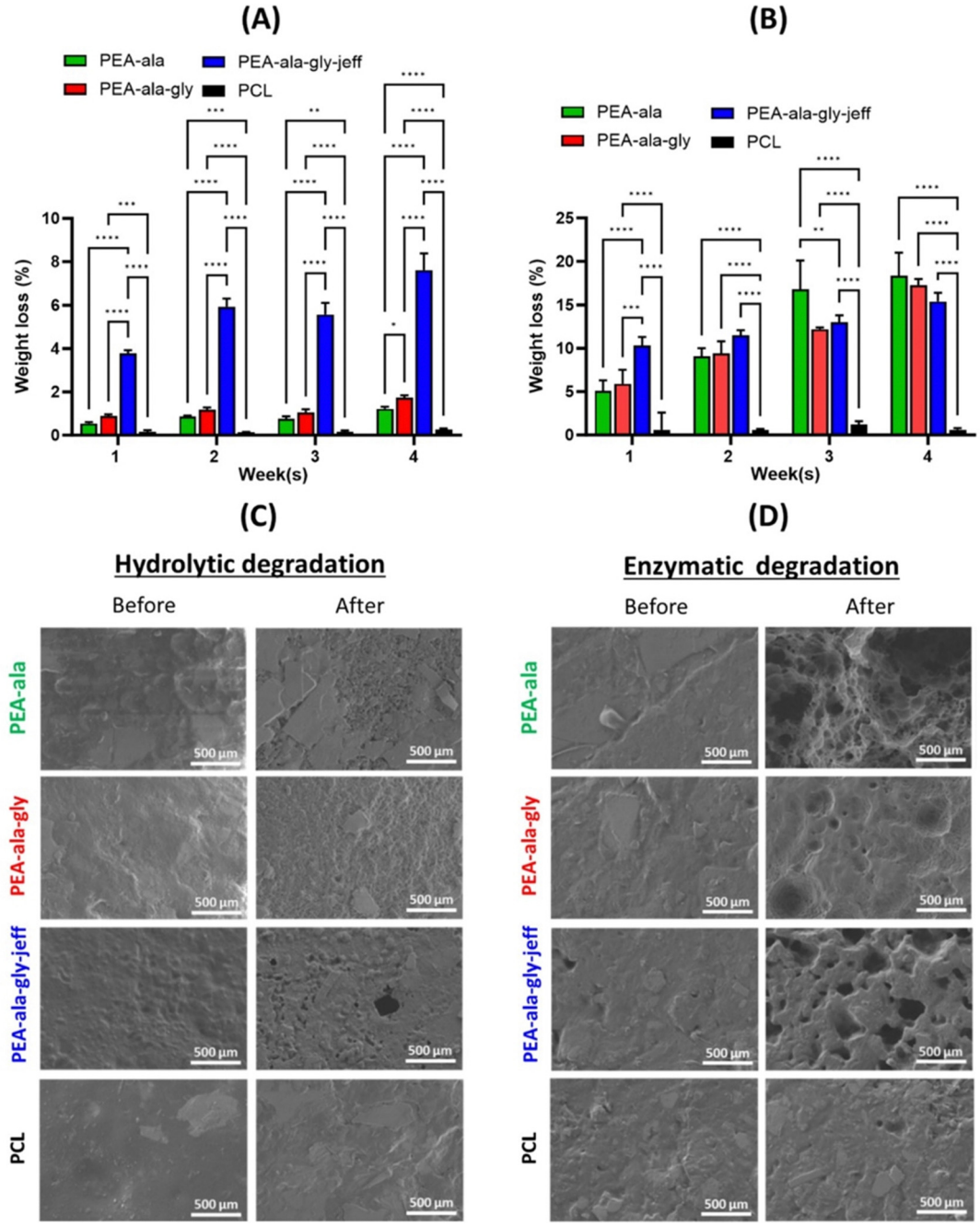

Fig. 8 Weight loss values for the AAA-PEAs and PCL films after 1, 2, 3 and 4 weeks in PBS (pH = 7.4), at 37 °C (A) and weight loss values for the AAA-PEAs and PCL films after 1, 2, 3 and 4 weeks in PBS containing α-chymotrypsin (from bovine pancreas) (0.4 mg mL^{-1}), (pH = 7.4), at 37 °C (B). Data are reported as mean value and error bar represents the standard deviation. Statistical analysis was performed using two-way ANOVA followed by Tukey's: (****) $p < 0.0001$, (***) $p < 0.001$, (**) $p < 0.01$, and (*) $p < 0.1$. SEM micrographs of AAA-PEAs and PCL surface films before and after *in vitro* hydrolytic (C) and enzymatic degradation (D).

applications. As depicted in Fig. 8(A), PEA-ala and PEA-ala–gly films exhibited similar and low values (<2%) of weight loss under hydrolytic conditions with no statistical differences except for week 4 ($p < 0.1$). The PEA-ala–gly–jeff films presented the highest, but still moderate, loss (7.6%) with a statistical difference ($p < 0.0001$) compared to the other AAA-PEAs and PCL-films. This increase in weight loss could be related to the higher hydrophilicity displayed by PEA-ala–gly–jeff films, increasing their affinity with the degradation medium and accelerating their degradation. As expected, the weight of PCL films remained almost unaltered throughout the duration of the study.

Weight loss of polymeric films in PBS (pH = 7.4) containing α-chymotrypsin is depicted in Fig. 8(B). In the presence of α-chymotrypsin, an enzyme usually involved in the inflammatory process of damaged tissues,[47] all AAA-PEAs show a gradual increase in weight loss over time with no statistical differences

between the different formulations except for week 1. Compared to hydrolytic degradation, the weight loss of AAA-PEAs films in week 1 is accelerated under enzymatic conditions (15–18%), with PEA-ala–gly–jeff presenting the highest value (*ca.* 10.3%) followed PEA-ala–gly (*ca.* 5.9%) and PEA-ala (*ca.* 5.1%). In a first stage (week 1), the more hydrophilic nature of PEA-ala–gly–jeff seems to favour its interaction with the enzymatic solution, accelerating its degradation compared to other AAA-PEAs. But as time progresses this trend is inverted and the differences completely attenuated by week 4. In turn, degradation kinetics of PCL films does not seem to be affected by the presence of the enzyme, displaying a profile similar to the hydrolytic one above. This phenomenon can be justified by the substrate specificity of the chosen enzyme (*i.e.* α-chymotrypsin) a protease that preferentially cleaves peptide amide bonds, present in the chemical structure of AAA-PEAs but not in PCL.

The surface morphology of the AAA-PEA and PCL films before and after *in vitro* hydrolytic and enzymatic degradation was analysed by SEM. Micrographs reported in Fig. 8(C) and (D) show a slight increase in surface roughness for all AAA-PEAs films after 4 weeks of incubation, suggesting their hydrolytic degradation *via* surface erosion. This effect is more evident in AAA-PEAs films containing jeff, likely due to their higher hydrophilicity. No significant surface alterations were detected in PCL films independently of the degradation media.

3.2.4 *In vitro* biological tests. The suitability of developed AAA-PEAs as biomaterials for TE applications was further investigated *in vitro* by assessing the viability, metabolic activity and morphology of hBM-MSCs seeded on top the polymeric films. Fluorescence microscopy images in Fig. 9(A) (top) confirm the ability of PEA-ala and PEA-ala–gly films to support the viability of hBM-MSC (in green) with a negligible number of dead cells (in red) 7 days post seeding, and comparable to both 2D control (tissue culture plate) and PCL films. The percentage of viable cells (Fig. 9(B)) remained high for all PEAs formulations (>95%) with no significant statistical differences observed, except for PEA-ala and plastic culture control (2D). Single plain confocal microscopy images (Fig. 9(A) bottom) taken after phalloidin F-actin and Hoechst 33342 labelling indicated that both PEA-ala and PEA-ala–gly materials were able to support the adhesion of cells with spindle-like shape typical of healthy hBM-MSCs.

Unfortunately, we were not able to detect the presence of cells on the surface of PEA-ala–gly–jeff films. This may have been caused by the pronounced changes in its surface features (see Fig. 8) compared to PEA-ala and PEA-ala–gly, resulting in cell detachment and subsequent loss during the washing phases required for the preparation of the films for biological tests.

Results obtained from direct contact test (Fig. 9(C)) showed an increased metabolic activity of hBM-MSCs over a period of 28 days, with comparable percentages of PrestoBlue™ reduction between AAA-PEA and PCL films. Through indirect contact it was not possible to detect significant differences in metabolic activity between cells seeded on PEA-ala–gly–jeff, PCL and other AAA-PEAs films, suggesting the absence of any cytotoxic compounds released from the films (Fig. 9(D)). These results agree with cell viability data and further confirm the suitability of all AAA-PEAs films to support the function of hBM-MSCs.

3.3 Fabrication and characterization of AAA-PEA scaffolds

3.3.1 Thermal analysis. As expected, processing of AAA-PEAs was challenging compared to PCL, mainly due to absence of crystallization and lower viscosity values (see DSC results in Fig. 5 and rheological data in Fig. S10, ESI†). To further investigate the thermal stability of the materials and potential degradation or property changes due to melt-extrusion processing, an isothermal TGA study was conducted at 100 °C (maximum processing temperature) for 10 hours (Fig. 10(A)). After 10–15 minutes at 100 °C, PEA-ala, PEA-ala–gly, and PEA-ala–gly–jeff exhibited weight losses of approximately 0.6%, 0.5%, and 0.9%, respectively. Under the same conditions, PCL showed a weight loss of only 0.1%. Notably, no further weight loss was observed after the initial reduction, indicating good thermal stability of the materials at relevant processing temperatures. The initial weight loss was likely due to moisture content, as AAA-PEAs and PCL absorb moisture differently based on their hydrophilicity. PCL, being less hydrophilic than the AAA-PEAs (as demonstrated by contact angle results in Section 3.2.3), absorbed less moisture and thus exhibited minimal weight loss. Among the AAA-PEAs, PEA-ala–gly–jeff, with the highest hydrophilicity, showed the greatest weight loss (0.9%), compared to 0.6% for PEA-ala and 0.5% for PEA-ala–gly.

To evaluate whether the printing process induced changes in the materials' thermal properties, a DSC analysis was performed on the fabricated scaffolds. The heat flow curve from the first heating run is presented in Fig. 10(B). The melting temperatures of the AAA-PEA scaffolds fall within the same range as those of the pristine materials before processing (50–100 °C, as shown in Section 3.1.2). In the case of the scaffolds, the melting peaks are better defined compared to the AAA-PEAs (Fig. 5), indicating a more organized crystalline structure.

The ΔH of the melting transition was determined for the scaffolds and compared to that of the AAA-PEAs after synthesis and purification (Table S8, ESI†). The values are very similar, indicating that the crystallinity of the scaffolds and pristine AAA-PEAs does not differ significantly. Similarly, for PCL, the melting temperature of the printed scaffold is comparable to that of unprocessed PCL, confirming that no significant thermal changes occurred as a result of melt-extrusion processing.

3.3.2 Morphology. Upon optimization of process parameters (Table S2, ESI†) it was possible to manufacture 3D scaffolds with well-organized structures and defined pore sizes/shapes, as well as a repeatable microstructure. SEM analysis (Fig. 10(C)) confirmed good coherence between experimental and theoretical values in terms of filament diameter (RW) and pore size (FG) (Table S6, ESI†). The small deviations observed (approx. 5%) in RW and FG can be attributed to slight variations in ambient temperature, which are difficult to control and can result in the heterogeneous solidification of extruded filaments. The 3D printed filaments appeared homogeneous and adequately fused over the entire cross-section of

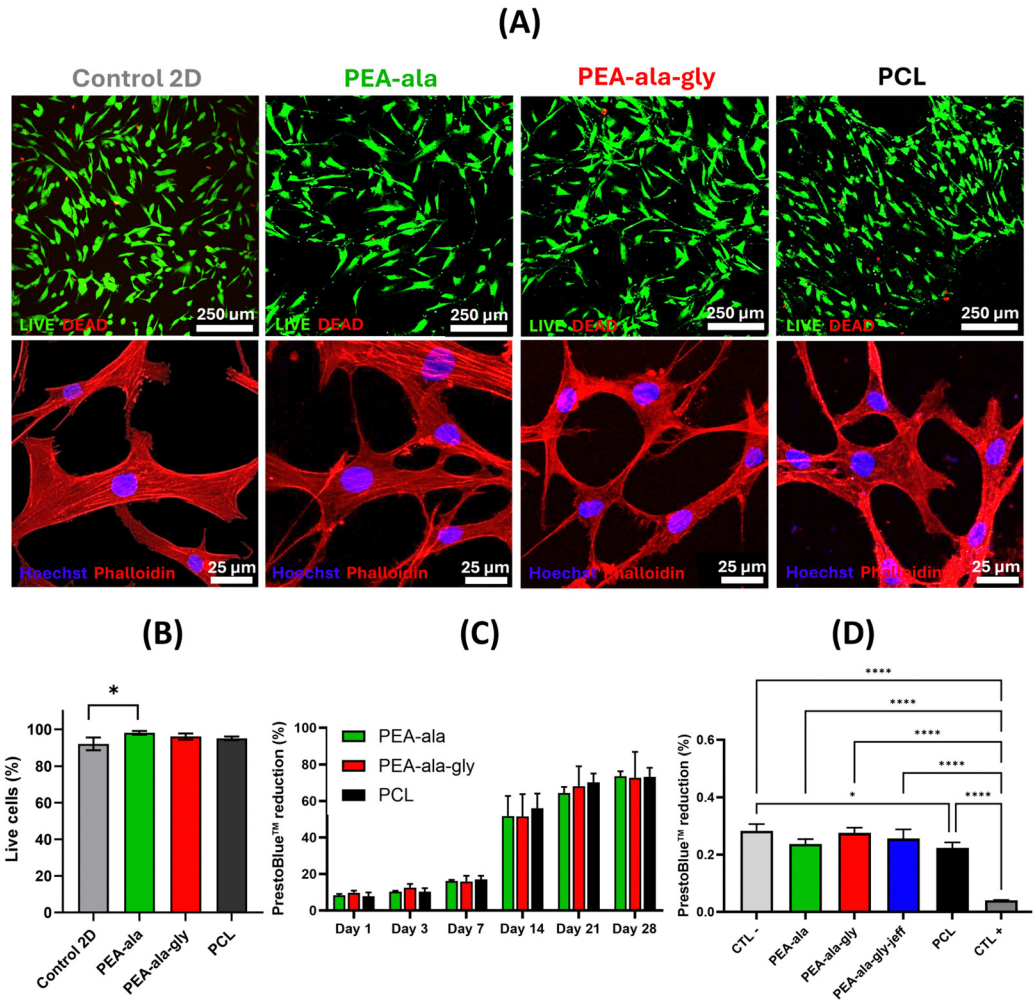

Fig. 9 Fluorescence confocal microscopy images of hBM-MCSs seeded onto AAA-PEAs and PCL films and stained with calcein-AM (live cells – green) and ethidium homodimer-1 (dead cells – red) (A) (top). Fluorescence confocal microscopy images of hBM-MCSs seeded onto AAA-PEA and PCL films and stained with phalloidin (F-actin – red) and Hoechst 33342 (nuclei – blue) (A) (bottom). A control 2D is still shown for each experiment. Mean ± standard deviation of live cells in percentage of three replicates after 7 days on PEAs and PCL films (B). Percentage of PrestoBlue™ reduction as a function of time for AAA-PEAs and PCL films (C). Percentage of PrestoBlue™ reduction of hBM-MSCs after 48 h expose to the media that was in contact with films of AAA-PEAs and PCL for 24 h. The negative control (CTL−) represents cells in cell culture media (with no treatment), the positive control (CTL+) represents cells in 1% Triton X-100 in cell culture media (D). Data are reported as mean and standard deviation. Statistical analysis was performed using one-way ANOVA followed by Tukey's. There was no statistical difference for direct method between the different films but there was for indirect method: (****) $p < 0.0001$ and (*) $p < 0.1$.

the scaffold, suggesting good structural stability. Regardless of the material, all constructs revealed a fully interconnected pore network (100%) with similar values for porosity (53–61%) and surface area to volume ratio (10–12 mm^{-1}), when analysed by micro-CT (Table S7, ESI†).

3.3.3 Mechanical compression tests. The stress–strain curves obtained for all 3D scaffolds (*i.e.*, PEA-ala, PEA-ala–gly, PEA-ala–gly–jeff, and PCL) are presented in Fig. 10(D). A linear region is easily recognizable at low strain values, indicating an initial stiff mechanical response. This zone is followed by a region of lower stiffness, and finally another stiff portion of the stress–strain curve could be noticed. This behavior has been reported several times for PCL 3D scaffolds obtained through fused deposition modeling.[16,25,29] The compressive modulus (E) was calculated as the slope of the initial linear region of the stress–strain curve. Fig. 10(E) shows the values of E and maximum stress (σ_{max}).

The values of compressive modulus and maximum stress for PCL scaffolds were 97 ± 9 MPa and 13.2 ± 0.7 MPa, respectively. However, the values for PEA-ala (55 ± 5 MPa and 9.4 ± 0.5 MPa), PEA-ala–gly (78 ± 8 MPa and 10.3 ± 0.5 MPa), and PEA-ala–gly-jeff scaffolds (42 ± 5 MPa and 5.0 ± 0.4 MPa) were significantly lower than those obtained for PCL scaffolds. In terms of compressive modulus and maximum stress, the observed differences were statistically significant. It is worth noting that the lowest value of the compressive modulus was found for PEA-ala–gly-jeff. This is likely to be related with the presence of ether linkages in its structure, causing an increase in the flexibility of the chains. The difference between the compressive Young's modulus of PEA-ala and PEA-ala–gly

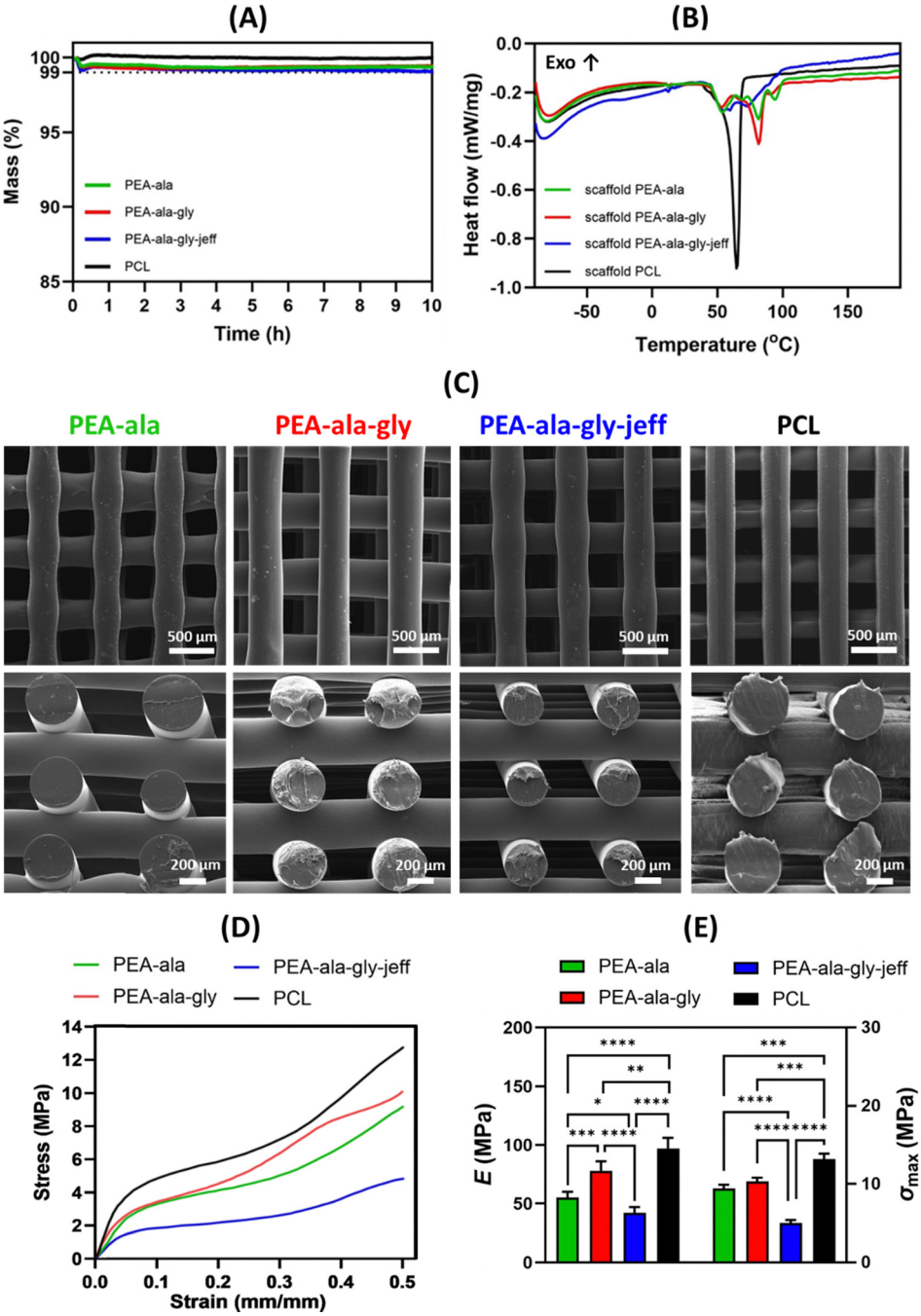

Fig. 10 Isothermal TGA of AAA-PEAs and PCL scaffolds performed at 100 °C for 10 hours (A). First heating DSC run of AAA-PEAs and PCL scaffolds carried out from −95 °C to 190 °C, at 5 K min^{-1} (B). SEM micrographs of 3D PCL and AAA-PEAs printed scaffolds: top view (up) and cross-section (bottom) (C). Typical stress–strain curves obtained from compression tests on 3D printed scaffolds (rate of 1 mm min^{-1}), final strain of 50% (D). Mechanical properties of PEA-ala, PEA-ala–gly, PEA-ala–gly-jeff, PCL scaffolds: compressive modulus (E) and maximum stress (σ_{max}) (E). The results are reported as mean value ± standard deviation. Statistical analysis was performed using two-way ANOVA followed by Tukey's: (****) $p < 0.0001$, (***) $p < 0.001$, (**) $p < 0.01$, and (*) $p < 0.1$.

scaffolds, may be related to the presence of glycine, which is an α-amino acid with a smaller lateral group than L-alanine, which can allow a greater packing of the chains, increasing the rigidity of the chains, and consequently the rigidity of the scaffold. The results from the compression tests showed that it is possible to change the mechanical behaviour of the 3D printed scaffolds, by changing the composition of AAA-PEAs.

Control of the process–structure–property relationship of a material plays a pivotal role in designing and developing 3D scaffolds with desired mechanical, biological, and functional properties. While this was outside the scope of the present work, it has been reported in detail in some of our previous studies.[17,18,25,29,48] In those studies, we demonstrated the role of material composition and material-design combinations,

particularly the effects of pore size and geometry (and consequently porosity), on the compressive mechanical performance and *in vitro* cell behavior through a systematic analysis of 3D scaffolds fabricated *via* extrusion-based additive manufacturing. The findings were supported by morphological analyses using SEM, micro-CT, and confocal laser scanning microscopy, which provided additional insights into the effects on functional features and cell morphology.

4. Conclusions

This study reports the synthesis and characterization of a new library of high molecular weight AAA-PEAs with tuneable physical, chemical and mechanical properties for scaffold-guided tissue regeneration. Despite their amorphous nature, AAA-PEAs demonstrated good thermal stability and suitable rheological properties for extrusion-based printing of 3D scaffolds with good shape fidelity and reproducibility. Changes in the chemical structure of the AAA-PEAs enabled the fabrication of 2D and 3D substrates with higher wettability, lower stiffness and faster degradation rates compared to PCL. However, these features did not seem to affect the behaviour of hBM-MSCs, which displayed similar levels of viability and metabolic activity independently of the substrate material. In summary, our study contributes to expand the range of processable materials *via* 3D printing and hints at the possibility of manipulating the structure of the AAA-PEAs to adjust the properties of engineered scaffolds to those of different tissues in the human body.

Abbreviations

2D	Two-dimensional
3D	Three-dimensional
AAA-PEAs	α-Amino acids based poly(ester amide)s
AM	Additive manufacturing
BAAD	Bis-α-(L-amino acid)-α,ω-alkylene diester
$CDCl_3$	Deuterated chloroform
DMF	*N*,*N*-Dimethylformamide
DMSO	Dimethyl sulfoxide
DMSO-d_6	Deuterated dimethy lsulfoxide
DMTA	Dynamic mechanical thermal analysis
DSC	Differential scanning calorimetry
FTIR	Fourier transform infrared spectroscopy
hBM-MSC	Human bone marrow mesenchymal stem cells
Jeff	Jeffamine
micro-CT	Micro-computed tomography
NHS	*N*-Hydroxysuccinimide
NMR	Nuclear magnetic resonance
PBS	Phosphate buffered saline
PCL	Poly(ε-caprolactone)
PEA	Poly(ester amide)
PEA-ala	L-Alanine based PEA
PEA-ala–gly	L-Alanine and glycine based PEA
PEA-ala–gly-jeff	L-Alanine, glycine and jeffamine based PEA
PLA	Poly(L-lactic acid)
PLGA	Poly(D,L-lactic-*co*-glycolic acid)
p-TSA	*p*-toluenesulfonic acid monohydrate
SE	Standard deviation of the mean
SEM	Scanning electronic microscopy
TE	Tissue engineering
TEA	Triethylamine
T_g	Glass transition temperature
TGA	Thermogravimetric analysis
TIPS	Thermally induced phase separation
WCA	Water contact angle

Author contributions

Patricia dos Santos: writing – original draft, visualization, software, methodology, investigation, formal analysis, data curation, conceptualization. Beatriz Alves: software, methodology, investigation, formal analysis. Sara Inocêncio: visualization, methodology, investigation, formal analysis. Pedro Nunes: visualization, methodology, investigation, formal analysis. Stephen M. Richardson: writing – review & editing, visualization, methodology, investigation, resources. Antonio Gloria: writing – review & editing, visualization, methodology, investigation, formal analysis. Arménio Serra: writing – review & editing, supervision, methodology, investigation, formal analysis. Ana Fonseca: writing – review & editing, validation, supervision, resources, project administration, methodology, investigation, funding acquisition, formal analysis, data curation, conceptualization. Marco Domingos: writing – review & editing, validation, supervision, resources, project administration, methodology, investigation, funding acquisition, formal analysis, data curation, conceptualization.

Data availability

Data will be made available on reasonable request to the corresponding authors.

Conflicts of interest

The authors declare that they have no known competing financial interests or personal relationships that could have appeared to influence the work reported in this paper.

Acknowledgements

Funding for Patricia dos Santos studentship was received from the Portuguese National Science Foundation through the FCT scholarship 2021.05900.BD. The authors would also like to thank the Henry Royce Institute EPSRC grants EP/R00661X/1, EP/S019367/1, EP/P025021/1 and EP/P025498/1. NMR data was obtained at the Nuclear Magnetic Resonance Laboratory of the Coimbra Chemistry Centre, facility which is supported in part by FEDER – European Regional Development Fund through the COMPETE Programme (Operational Programme for Competitiveness) and by National Funds through FCT through grants

REEQ/481/QUI/2006, RECI/QEQ-QFI/0168/2012, CENTRO-07-CT62-FEDER-002012, and Rede Nacional de Ressonância Magnética Nuclear (RNRMN). This research is sponsored by FEDER funds through the program COMPETE – Programa Operacional Factores de Competitividade – and by national funds through FCT under the project UID/EMS/00285/2020 and LA/P/0112/2020. The authors would like to thank Dr Jen Adcott, Dr Pauline Baird and Dr Miley Li from the University of Manchester for the technical support provided during 3D printing, cell culture and bioimaging activities.

References

1 H. S. Kim, S. G. Kumbar and S. P. Nukavarapu, *Curr. Opin. Biomed. Eng.*, 2021, **17**, 100260.
2 A. C. Fonseca, F. P. W. Melchels, M. J. S. Ferreira, S. R. Moxon, G. Potjewyd, T. R. Dargaville, S. J. Kimber and M. Domingos, *Chem. Rev.*, 2020, **120**, 11093–11139.
3 M. Vahidi, A. S. Rizkalla and K. Mequanint, *Adv. Healthcare Mater.*, 2024, **13**, e2401218.
4 S. Wang, S. Hashemi, S. Stratton and T. L. Arinzeh, *Adv. Healthcare Mater.*, 2021, **10**, e2001244.
5 J. Chi, M. Wang, J. Chen, L. Hu, Z. Chen, L. J. Backman and W. Zhang, *Biomimetics*, 2022, **7**, 131.
6 M. Krishani, W. Y. Shin, H. Suhaimi and N. S. Sambudi, *Gels*, 2023, **9**, 100.
7 I. M. Adel, M. F. ElMeligy and N. A. Elkasabgy, *Pharmaceutics*, 2022, **14**, 306.
8 A. Kumar and A. Jacob, *J. Appl. Biol. Biotechnol.*, 2022, **10**, 163–176.
9 G. H. Wu and S. H. Hsu, *J. Med. Biol. Eng.*, 2015, **35**, 285–292.
10 L. G. Bracaglia, B. T. Smith, E. Watson, N. Arumugasaamy, A. G. Mikos and J. P. Fisher, *Acta Biomater.*, 2017, **56**, 3–13.
11 J. K. Placone and A. J. Engler, *Adv. Healthcare Mater.*, 2018, **7**, e1701161.
12 S. Tian, H. Zhao and N. Lewinski, *Bioprinting*, 2021, **23**, e00156.
13 T. T. Brink, F. Damanik, J. I. Rotmans and L. Moroni, *Adv. Healthcare Mater.*, 2024, **13**, e2301939.
14 S. Vach Agocsova, M. Culenova, I. Birova, L. Omanikova, B. Moncmanova, L. Danisovic, S. Ziaran, D. Bakos and P. Alexy, *Materials*, 2023, **16**, 4267.
15 S. Castañeda-Rodríguez, M. González-Torres, R. M. Ribas-Aparicio, M. L. Del Prado-Audelo, G. Leyva-Gómez, E. S. Gürer, J. Sharifi-Rad, S. Castañeda-Rodríguez, M. González-Torres, R. M. Ribas-Aparicio, M. L. Del Prado-Audelo, G. Leyva-Gómez, E. S. Gürer and J. Sharifi-Rad, *J. Biol. Eng.*, 2023, **17**, 21.
16 M. Domingos, F. Intranuovo, A. Gloria, R. Gristina, L. Ambrosio, P. J. Bartolo and P. Favia, *Acta Biomater.*, 2013, **9**, 5997–6005.
17 M. Domingos, A. Gloria, J. Coelho, P. Bartolo and J. Ciurana, *Proc. Inst. Mech. Eng., Part H*, 2017, **231**, 555–564.
18 S. Cometa, M. A. Bonifacio, E. Tranquillo, A. Gloria, M. Domingos and E. De Giglio, *Polymers*, 2021, **13**, 150.
19 H. Wang, M. Domingos and F. Scenini, *Rapid Prototyp. J.*, 2018, **24**, 731–738.
20 A. C. Fonseca, M. H. Gil and P. N. Simões, *Prog. Polym. Sci.*, 2014, **39**, 1291–1311.
21 K. Ghosal, M. S. Latha and S. Thomas, *Eur. Polym. J.*, 2014, **60**, 58–68.
22 A. Rodriguez-Galan, L. Franco, J. Puiggali, A. Rodriguez-Galan, L. Franco and J. Puiggali, *Polymers*, 2010, **3**, 65–99.
23 S. R. Moxon, M. J. S. Ferreira, P. d Santos, B. Popa, A. Gloria, R. Katsarava, D. Tugushi, A. C. Serra, N. M. Hooper, S. J. Kimber, A. C. Fonseca, M. A. N. Domingos, S. R. Moxon, M. J. S. Ferreira, P. d Santos, B. Popa, A. Gloria, R. Katsarava, D. Tugushi, A. C. Serra, N. M. Hooper, S. J. Kimber, A. C. Fonseca and M. A. N. Domingos, *Polymers*, 2020, **12**, 1478.
24 V. Ansari, A. Calore, J. Zonderland, J. A. W. Harings, L. Moroni and K. V. Bernaerts, *Biomacromolecules*, 2022, **23**, 1083–1100.
25 A. Gloria, B. Frydman, M. L. Lamas, A. C. Serra, M. Martorelli, J. F. J. Coelho, A. C. Fonseca and M. Domingos, *Mater. Sci. Eng., C*, 2019, **98**, 994–1004.
26 E. Chkhaidze, D. Tugushi, D. Kharadze, Z. Gomurashvili, C.-C. Chu and R. Katsarava, *J. Macromol. Sci., Part A: Pure Appl. Chem.*, 2011, **48**, 7064–7123.
27 G. Tsitlanadze, T. Kviria, R. Katsarava and C. C. Chu, *J. Mater. Sci.: Mater. Med.*, 2004, **15**, 185–190.
28 S. Strassburg, S. M. Richardson, A. J. Freemont and J. A. Hoyland, *Regener. Med.*, 2010, **5**, 701–711.
29 M. Domingos, F. Intranuovo, T. Russo, R. D. Santis, A. Gloria, L. Ambrosio, J. Ciurana and P. Bartolo, *Biofabrication*, 2013, **5**, 045004.
30 V. Andrés-Guerrero, M. Zong, E. Ramsay, B. Rojas, S. Sarkhel, B. Gallego, R. d Hoz, A. I. Ramírez, J. J. Salazar, A. Triviño, J. M. Ramírez, E. M. d Amo, N. Cameron, B. de-las-Heras, A. Urtti, G. Mihov, A. Dias and R. Herrero-Vanrell, *J. Controlled Release*, 2015, **211**, 105–117.
31 H. Sun, R. Cheng, C. Deng, F. Meng, A. A. Dias, M. Hendriks, J. Feijen and Z. Zhong, *Biomacromolecules*, 2015, **16**, 597–605.
32 C. Boyer, J. Liu, L. Wong, M. Tippett, V. Bulmus and T. P. Davis, *J. Polym. Sci., Part A: Polym. Chem.*, 2008, **46**, 7207–7224.
33 Y. Fan, M. Kobayashi and H. Kise, *J. Polym. Sci., Part A: Polym. Chem.*, 2001, **39**, 1318–1328.
34 M. Deng, J. Wu, C. A. Reinhart-King and C.-C. Chu, *Biomacromolecules*, 2009, **10**, 3037–3047.
35 P. Ranganathan, C.-W. Chen, S.-P. Rwei, Y.-H. Lee and S. K. Ramaraj, *Polym. Degrad. Stab.*, 2020, **181**, 109323.
36 A. Soleimani, S. Drappel, R. Carlini, A. Goredema and E. R. Gillies, *Ind. Eng. Chem. Res.*, 2014, **53**, 1452–1460.
37 M. L. Lamas, M. S. Lima, A. C. Pinho, D. Tugushi, R. Katsarava, E. C. Costa, I. J. Correia, A. C. Serra, J. F. J. Coelho and A. C. Fonseca, *Polymer*, 2018, **150**, 343–359.
38 A. Galarza Torre, J. E. Shaw, A. Wood, H. T. J. Gilbert, O. Dobre, P. Genever, K. Brennan, S. M. Richardson,

J. Swift, A. Galarza Torre, J. E. Shaw, A. Wood, H. T. J. Gilbert, O. Dobre, P. Genever, K. Brennan, S. M. Richardson and J. Swift, *Sci. Rep.*, 2018, **8**, 8981.
39 S. Cho, J. Irianto and D. E. Discher, *J. Cell Biol.*, 2017, **216**, 305–315.
40 A. Athirasala, N. Hirsch and A. Buxboim, *Curr. Opin. Cell Biol.*, 2017, **46**, 119–127.
41 B. D. Matthews, C. K. Thodeti, J. D. Tytell, A. Mammoto, D. R. Overby and D. E. Ingber, *Integr. Biol.*, 2010, **2**, 435–442.
42 Y. Lu, D. Cheng, B. Niu, X. Wang, X. Wu and A. Wang, *Pharmaceuticals*, 2023, **16**, 454.
43 L. Bacakova, E. Filova, M. Parizek, T. Ruml and V. Svorcik, *Biotechnol. Adv.*, 2011, **29**, 739–767.
44 W. Xie, X. Wei, H. Kang, H. Jiang, Z. Chu, Y. Lin, Y. Hou and Q. Wei, *Adv. Sci.*, 2023, **10**, 2204594.
45 Q. Wei, S. Wang, F. Han, H. Wang, W. Zhang, Q. Yu, C. Liu, L. Ding, J. Wang, L. Yu, C. Zhu and B. Li, *Biomater. Transl. Med.*, 2021, **2**, 323–342.
46 S. Nellinger and P. J. Kluger, *Int. J. Mol. Sci.*, 2023, **24**, 3551.
47 D. Shah, K. Mital, D. Shah and K. Mital, *Adv. Ther.*, 2017, **35**, 31–42.
48 J. Ferreira, A. Gloria, S. Cometa, J. F. Coelho and M. Domingos, *J. Appl. Biomater. Biomech.*, 2017, **15**, 185–195.

